PERGAMON

International Journal of Heat and Mass Transfer 42 (1999) 4391–4409

International Journal of HEAT and MASS TRANSFER

www.elsevier.com/locate/ijhmt

Test of several versions for the k–ε type turbulence modelling of internal mixed convection flows

J.J. Costa [a,*], L.A. Oliveira [a], D. Blay [b]

[a] *Departmento de Engenharia Mecânica, Universidade de Coimbra—Polo II, 3030 Coimbra, Portugal*
[b] *Laboratoire d'Etudes Thermiques, E.N.S.M.A.—BP 109, 86960 Futuroscope Cedex, France*

Received 27 July 1998; received in revised form 25 January 1999

Abstract

The problem of confined, mixed convection airflow generated by two non-isothermal plane wall jets was investigated numerically and experimentally. Measurements of the velocity and temperature fields in a 1×1 m^2 cross-section cavity are reported. Eight low-Reynolds-number k–ε turbulence models were comparatively tested, together with a simplified version of the two-layer wall-function model of Chieng and Launder. Particular attention was given to the mean and turbulent quantities across the wall jet flows, and to the evaluation of the wall heat transfer. The low-*Re* model of Nagano and Hishida provided satisfactory results, which were still improved with two further modifications.

1. Introduction

The numerical simulation of air flow and heat transfer processes is presently a most valuable method of analysis for the design of indoor environments. Provided the pertinent approximations and boundary conditions are properly used, the accuracy of the numerical approach relies mainly on the ability of the associated turbulence model to reproduce the turbulent features of momentum and heat transport.

As reviewed by Chen and Jiang [1], the *standard* k–ε turbulence model [2] has been widely used to study the field distributions of air velocity, temperature, turbulence intensity, relative humidity, contaminant concentration and the air quality within ventilated rooms. Yielding reasonable results in many applications, it became most attractive for engineers in this field, since it is easy to program and generally ensures a robust and convergent behaviour of the calculation procedure. However, this model should be restricted to regions of fully turbulent flow, while the near-wall layers of viscous-affected flow are bridged by the use of logarithmic wall-functions. These functions stand on the assumption of attached boundary-layer or channel flows, therefore lacking the theoretical basis to be applied in the prediction of separating, reattaching or recirculating turbulent flows. Nevertheless, such high-turbulence-Reynolds-number formulation of the k–ε model has been frequently used and critically evaluated in the numerical prediction of convective heat transfer in complex turbulent flows, either with the standard, or with improved or ad hoc modified wall-functions [3–6]. In contrast with what has been commonly accepted, predictions with the high-*Re* k–ε model can be significantly improved in certain complex flow problems, provided that wall-refined grids are used together with two- or three-layer wall-functions [7].

In many situations of room ventilation, velocities

* Corresponding author. Tel.: +351-39-790714; fax: +351-39-790701.

0017-9310/99/$ - see front matter
PII: S0017-9310(99)00075-7

Nomenclature

A	test cavity half-width [m]
B	width of guard cavities [m]
$C_{\varepsilon 1}, C_{\varepsilon 2}, C_{\varepsilon 3}, C_\mu$	constants of turbulence model
d, d_j	jet slot width [m]
D_k, E_ε	extra-terms in the k and ε equations
f_μ, f_1, f_2	functions of low-Re k–ε models
Fr_g	global Froude number $\{=U_c/[g\beta H(T_o-T_h)]^{1/2}\}$
Fr_j	jet Froude number $\{=U_j/[g\beta d_j(T_v-T_h)]^{1/2}\}$
g_i	gravitational acceleration in the i-direction [m s^{-2}]
G_k	rate of buoyancy production/destruction of turbulence kinetic energy [m^2 s^{-3}]
H	height of the cavity [m]
H^*	height of the left wall ($=H-d_h$) [m]
I_t	turbulence intensity $\{=[(\overline{u'^2}+\overline{v'^2})/2]^{1/2}/U_c$, from measurements; or $=(2k/3)^{1/2}/U_c$, from calculations$\}$
k	turbulence kinetic energy ($=\overline{u_i'u_i'}/2$) [m^2 s^{-2}]
L	length of the cavity [m]
L_c	characteristic length ($=d_h+d_v$) [m]
$\dot{m}$	mass flow rate [kg s^{-1}]
$\overline{Nu}_y$	local Nusselt number on the left wall
$\overline{Nu}_{Left}$	average Nu number on the left wall: $\overline{Nu}_{Left}=\frac{1}{H^*}\int_0^{H^*} Nu_y\,dy$; $Nu_y=\left\lvert -\frac{H}{\Delta T_v}\frac{\partial T}{\partial x}\right\rvert_{x=0}$
p	pressure [N m^{-2}]
p_{ef}	$=p+2/3\times\rho k$, for numerical convenience [N m^{-2}]
P_k	rate of shear production of k [m^2 s^{-3}]
Pr/Pr_t	molecular/turbulent Prandtl number
Re_g	global Reynolds number ($=U_cL_c/\nu$)
Re_j	jet Reynolds number ($=U_jd_j/\nu$)
Re_n	turbulence Reynolds number ($=k^{1/2}x_n/\nu$)
Re_t	local-turbulence Reynolds number ($=k^2/\nu\tilde{\varepsilon}$)
$S_1,\ldots S_5$	monitoring locations (cf. Fig. 1(b))
S_ϕ	source-term in the differential Eq. (1)
T	temperature [°C]
T_{ref}	reference temperature $[=(T_h+T_v)/2]$ [°C]
u, v	mean velocity components (cf. Fig. 1(b)) [m s^{-1}]
u_i	mean velocity in the i-direction [m s^{-1}]
u_m, v_m	average values of velocity profiles [m s^{-1}]
u_τ	friction velocity $[=(\tau_w/\rho)^{1/2}]$ [m s^{-1}]
U_c	characteristic velocity scale $\{=(U_hd_h+U_vd_v)/(d_h+d_v)\}$ [m s^{-1}]
U_h (U_v)	horizontal (vertical) jet velocity [m s^{-1}]
U_{rm}	maximum velocity in the return flow [m s^{-1}]
$\dot{v}$	jet discharge airflow rate [m^3 s^{-1}]
$\dot{V}$	airflow rate in the closed circuit (cf. Fig. 2) [m^3 s^{-1}]
x, y	spatial coordinates (cf. Fig. 1) [m]
x_n	normal distance to the nearest wall [m]
x_n^+	dimensionless wall-distance ($=u_\tau x_n/\nu$).

Greek symbols

α	molecular thermal diffusibility [m^2 s^{-1}]
α_t	turbulent thermal diffusibility [m^2 s^{-1}]
β	thermal expansion coefficient [K^{-1}]
ΔT_v	characteristic temperature ??difference ($=T_v-T_h$)
ε, $\tilde{\varepsilon}$	dissipation rate of k ($\tilde{\varepsilon}=\varepsilon+D_k$) [m^2 s^{-3}]
ϕ	generic variable
Γ_ϕ	diffusibility in mean-flow equations
κ	von Karman constant ($=0.4187$)
ν	molecular kinematic viscosity [m^2 s^{-1}]
ν_t	turbulent kinematic viscosity [m^2 s^{-1}]
μ	fluid dynamic viscosity ($=\rho\nu$) [N s m^{-2}]
Θ	dimensionless temperature $[=(T-T_h)/(T_v-T_h)]$
ρ	fluid density [kg m^{-3}]
σ_k, σ_ε	constants of turbulence model
τ_t	turbulent shear stress ($=-\rho\overline{u'v'}$) [N m^{-2}]
τ_w	wall shear stress $\{=\mu(du/dx_n)_w\}$ [N m^{-2}]
ψ	stream function [m^2 s^{-1}] (dimensionless: $\Psi=\psi/(U_cL_c)$).

Superscripts

$'$	fluctuating quantity
$+$	dimensionless wall variables.

Subscripts

h	horizontal jet
in	inlet condition
i, j	spatial indices
j	generic jet
n	direction normal to a surface
out	outlet condition
t	turbulent
v	vertical jet
w	wall condition
1	first inner grid point.

are small and wall-bounded flow layers are neither fully turbulent and well developed, nor completely laminar. Turbulence models that account for low-Reynolds-number and near-wall turbulence decay effects should therefore be considered. During the last two decades, over a dozen different proposals of 'low-*Re*' (or 'near-wall') tXurbulence models, mostly of the k–ε type, have been published and extensively tested in a variety of isothermal boundary layer problems [8], as well as in natural [9–12] and forced convection flow configurations [13,14]. The application of such models to mixed convection internal flows has however been scarcer [15], particularly within the low velocity and turbulence limits that are presently imposed by thermal comfort requirements in room ventilation [16,17].

In a previous work by the authors [18], the two-dimensional recirculating flow generated by two non-isothermal low-velocity wall jets inside a cavity was investigated both experimentally and numerically for one parameter configuration in a mixed convection regime. The physical model can be classified as a mixing flow ventilation system, where fresh air is horizontally injected adjacent to the ceiling and heat is supplied by a warm vertical wall jet at the floor level. The velocity and temperature measurements obtained from a laboratory set-up were used for a preliminary validation of three different turbulence models, namely the *standard* high-*Re* k–ε model [2] with the two-layer wall-functions and the low-*Re* k–ε models of Jones and Launder [19,20] and its modified version by Launder and Sharma [21]. Somehow surprisingly, since it is not conceptually recommended for the prediction of low turbulence flows or to be used with a near-wall refined grid, the former performed globally better than the two latter.

The present study retrieves a direct sequence of that work [22], by further exploring several other versions of the low-*Re* κ–ε turbulence model, five of which were recently used by Hsieh and Chang [14] to study wall heat transfer problems in pipe-expansion flows. The 'near-wall model for high-Reynolds-numbers' of Chieng and Launder [3], incorporating a simplified, yet consistent formulation of two-layer wall-functions, is also used in the same near-wall refined grid. Numerical results are presented for the two-jet flow problem that was experimentally investigated by the present authors (*test-case*), as well as for two further mixed convection flow configurations that are documented in the literature. With reference to the experimental data, the performance of the different turbulence models is assessed, mainly by comparing the predicted profiles at some representative locations in the flow domain.

2. Experimental apparatus and procedure

2.1. Laboratory assembly and experimental model

The experimental apparatus was designed so as to generate two-dimensional flow and temperature fields, in order to provide a laboratory reference for validation of corresponding two-dimensional calculation procedures.

Experiments were performed on a laboratory model composed of a $1040 \times 1040 \times 700$ mm cavity equipped with two inlet slots (20 mm wide) and one outlet slot (24 mm wide), as sketched in Fig. 1(a). This cavity was divided into three identical smaller ones, the central working cavity (300 mm wide), where measurements were performed, and two side cavities (200 mm wide each), where flow and temperature fields similar to those in the working cavity were reproduced. The inlet slots allowed the discharge of two perpendicular air jets into the model: the warm air vertical wall jet at the floor level, and the cold air horizontal wall jet beneath the ceiling, both at the coordinate $x/L = 0$.

Every wall of dimensions $L \times H$ (parallel to the xOy plane) was made of transparent 1.5 mm plexiglass, thus providing a wide optical access to the test section. The two walls separating the central from the guard cavities were considered to be adiabatic. Each of the four thermally active walls ($x/L = 0$ and 1, $y/H = 0$ and 1) was built up with hollow rulers of polished aluminium and acted as an independent flat heat exchanger, maintained at a constant and uniform temperature by the use of controlled temperature water which flowed in a chicane circuit. The water flow rate was oversized to ensure that no significant temperature gradient could prevail anywhere on the wall surface. Under these conditions, the imposed wall surface temperature could be chosen between 10 and 50°C with a precision of 0.25°C. A 15 mm wide slot was provided at the top wall ($y/H = 1$) for the passage of a temperature probe and its displacement in a xOy plane. At the $x/L = 1$ vertical wall, a narrow glass window allowed the introduction of a light sheet for flow visualization in the test cavity.

Care was taken to ensure that variations of the flow and thermal fields in the spanwise direction were reduced to the lowest possible values. Unfortunately, this was only partially achieved. As reported in Section 5, some three-dimensional effects were always detected, which were mainly due to the interaction of the horizontal and vertical jets. Exploratory tests on the dynamic field were performed in a cavity with the whole width of the model (700 mm) but similar 3D effects were still observed. The presence of the guard cavities is thus justified only by thermal arguments.

The laboratory assembly is schematically represented in Fig. 2, where the different subsystems can be ident-

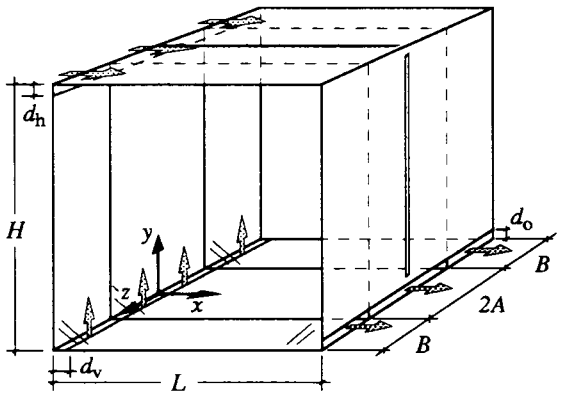

(a)

H	L	$d_h=d_v$	d_o	2A	B
1040	1040	20	24	300	200

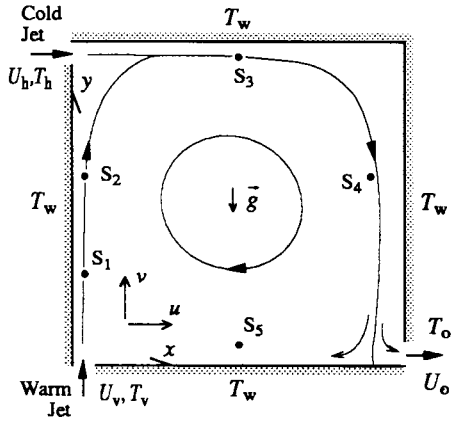

(b)

	S_1	S_2	S_3	S_4	S_5
x/L	0.0385	0.0385	0.5	0.865	0.5
y/H	0.288	0.596	0.962	0.596	0.0577

Fig. 1. (a) Configuration and dimensions (in mm) of the experimental model and the coordinate system adopted. (b) Sketch of the flow geometry in the test cavity cross section and different locations S_1–S_5 selected for monitoring purposes.

ified: the experimental model, the LDA system with its optical and electronic arrangements, one of the water circuits for the temperature control in the thermally active walls, and one (of the two identical) air circuits. In each of these, the air was made to circulate in a closed circuit, going through a water–air heat exchanger at a rate $\dot{V}$ significantly greater than that of the respective jet discharge, $\dot{v}$, thus creating the necessary inertia for reasonable stability and uniformity of the air velocity and temperature distributions along the jet slot. Filtered ambient air for both circuits was taken into a common mixing chamber, where it was seeded with fine oil particles, as required for LDA measurements. The mean jet velocity was varied and controlled by means of a manual valve and a calibrated Pitot tube. The air for injection was made to pass through a porous medium and a honeycombed structure in order to provide uniform velocity along each jet slot. Preliminary measurements made on the free jet issuing from each slot (before fitting up in the cavity) verified that the two-dimensionality of the mean axial velocity and temperature profiles taken along the slot centerline was within ± 6 and 0.5% of the respective mean values.

Velocity measurements were performed with a two-component laser-Döppler anemometer, in a differential mode and forward scattering configuration which allowed to measure simultaneously both the horizontal and the vertical time-mean velocity components projected on a xOy plane and the respective mean square fluctuations. The local air temperature was measured with a calibrated 25 μm K-type thermocouple probe that could sweep a xOy plane in the central cavity.

Both the LDA optical device and the temperature probe were moved by means of two independent micrometric displacement devices, which ensured a positioning error lower than 1 mm. The size of the laser beam control volume was 0.15×1 mm. Electronic noise was eliminated by filtering. The nominal accuracy of the measurement systems was 5% for both velocity components and 0.1°C for the temperature. The deviation from isothermality of the walls was lower than 0.2°C (difference between the water inlet and outlet temperatures).

3. Numerical method

The flow configuration studied is schematically represented in Fig. 1(b). To simplify the problem, the confined turbulent airflow was considered to be two-dimensional, incompressible, steady-state in mean and the Boussinesq approximation [23] was assumed for the fluid physical properties.

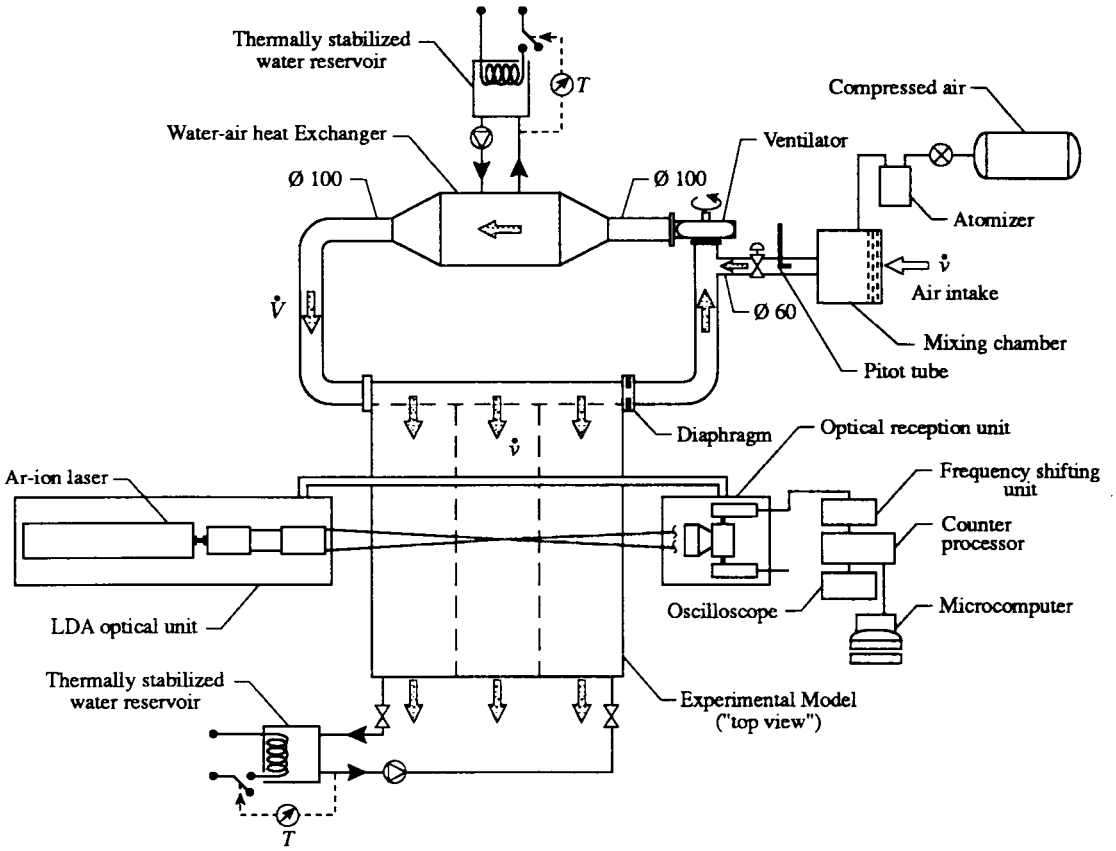

Fig. 2. Schematic diagram of the experimental assembly.

3.1. Mean flow and turbulence modelling equations

The flow simulation procedure is based on the solution of the finite-difference time-averaged equations expressing the conservation of mass, momentum and thermal energy. Turbulent fluxes are modelled under the assumption of turbulent diffusivities, thus implying the solution of two further transport equations for the turbulent kinetic energy, k, and its dissipation rate, ε (or $\tilde{\varepsilon}$, as will be seen below). Together with the usually called Prandtl–Kolmogorov relation for the turbulent viscosity, $\nu_t = f_\mu C_\mu k^2/\tilde{\varepsilon}$, they form a complete set of equations and can be reduced to the general form (cf. Nomenclature for further symbol identification):

$$\frac{\partial}{\partial x_j}(u_j\phi) = \frac{\partial}{\partial x_j}\left(\Gamma_\phi \frac{\partial \phi}{\partial x_j}\right) + S_\phi, \tag{1}$$

where the diffusibility Γ_ϕ and the source-term S_ϕ take the different meanings indicated in Table 1, according to the dependent variable represented by ϕ.

The terms P_k and G_k in the k and ε equations represent, respectively, the rates of shear production and buoyancy production/destruction of turbulence energy. They are modelled by:

$$P_k = \nu_t\left(\frac{\partial u_i}{\partial x_j} + \frac{\partial u_j}{\partial x_i}\right)\frac{\partial u_i}{\partial x_j} \tag{2}$$

$$G_k = g_j\beta\frac{\nu_t}{Pr_t}\frac{\partial T}{\partial x_j} \tag{3}$$

As specified in Table 1, the transport equations are written in the low-*Re* form of the k–ε model, extended to account for buoyancy effects on the turbulence production/destruction by the addition of terms with G_k in the k and ε equations. They differ from their basic version in the high-*Re* model [2] by the inclusion of (i) the viscous diffusion terms in all transport equations, (ii) the modifying functions f that make the terms containing constants C dependent upon the local level of turbulence and, in some cases, (iii) additional terms denoted by D_k and E_ε to better represent the near-wall behaviour of turbulence. Also, the use of $\tilde{\varepsilon} = \varepsilon + D_k$ as the 'dissipation variable' is here adopted for generality

Table 1
Values of Γ_ϕ and S_ϕ in the general transport Eq. (1)

Transported property	ϕ	Γ_ϕ	S_ϕ
Mass	1	0	0
Momentum in i-direction	u_i	$\nu_{\text{ef}} = \nu + \nu_{\text{t}} = \nu + f_\mu C_\mu \frac{k^2}{\tilde{\varepsilon}}$	$-\frac{1}{\rho}\frac{\partial p_{\text{ef}}}{\partial x_i} - g_i\beta(T - T_{\text{ref}}) + \frac{\partial}{\partial x_j}(\nu_{\text{ef}}\frac{\partial u_j}{\partial x_i})$
Thermal energy	T	$\alpha_{\text{ef}} = \frac{\nu}{Pr} + \frac{\nu_{\text{t}}}{Pr_{\text{t}}}$	0
Turbulent kinetic energy	k	$\nu + \frac{\nu_{\text{t}}}{\sigma_k}$	$P_k + G_k - \tilde{\varepsilon} + D_k$
Dissipation rate of k	$\tilde{\varepsilon}$	$\nu + \frac{\nu_{\text{t}}}{\sigma_\varepsilon}$	$\frac{\tilde{\varepsilon}}{k}(f_1 C_{\varepsilon 1} P_k - f_2 C_{\varepsilon 2}\tilde{\varepsilon} + C_{\varepsilon 1} C_{\varepsilon 3} G_k) + E_\varepsilon$

and for the computational convenience of taking $\tilde{\varepsilon} = 0$ at the wall.

3.2. Boundary conditions

3.2.1. Jet inlet conditions

Local values of the measured profiles were assigned to the velocity components u and v and temperature T at both jet inlet sections, using conveniently fitted polynomial functions; k and ε were specified via

$$k_{\text{in}} = 1.5 I_{\text{t}_{\text{in}}}^2 U_{\text{c}}^2 \tag{4}$$

$$\tilde{\varepsilon}_{\text{in}} = k_{\text{in}}^{3/2}/L_\varepsilon \tag{5}$$

respectively, where $I_{\text{t}_{\text{in}}}$ $\{=[(\overline{u'^2}+\overline{v'^2})/2]^{1/2}/U_{\text{c}}\}$ means the local turbulence intensity profile measured for each jet (j) and L_ε is a length scale for dissipation, taken here as $d_{\text{j}}/2$.

By exploratory calculations for the test-case configuration ($Re_{\text{j}} \approx 700$, see Section 5.1), it was verified that, for levels of $I_{\text{t}_{\text{in}}} < 10\%$, the flow field solutions were rather insensitive to the assumed distributions and precise values of k and ε at the inlet sections. In fact, the transport equations of those variables are source-term dominated, and the global level of turbulence intensity in the flow domain is mainly established by the strong shear production of k in the early mixing layer of the jets. In contrast, the shape of the streamwise velocity inlet profiles was observed to significantly affect the growth of the jets and the local wall heat transfer rate up to a distance of 25 to 30 slot widths.

3.2.2. Exit conditions

Zero normal gradients were specified at the exit section for all variables, except for u which was iteratively specified to ensure overall mass balance, on the basis of the mass flow rate evaluated at the row of upstream-neighbour nodes (ni−1):

$$u_{\text{ni, j}} = u_{\text{ni}-1,\text{ j}} \times f_u, \quad j = j_{\text{out}_1}, \ldots, j_{\text{out}_2} \tag{6}$$

where

$$f_u = \frac{\dot{m}_{\text{in}}}{\dot{m}_{\text{out,ni}-1}}, \quad \text{with} \quad \dot{m}_{\text{out,ni}-1} = \left(\int_0^{d_{\text{o}}} \rho u \, \text{d}y\right)_{x=L-\delta x} \approx \rho \sum_{j_{\text{out}_1}}^{j_{\text{out}_2}} (u_{\text{ni}-1,\text{j}} \times \Delta y_{\text{j}}).$$

In spite of the remarkable changes of the flow properties in the close vicinity of the outlet section, the use of these exit conditions did ensure physical realism of the results and provided a good convergence rate of the computations. This is due to the very small grid spacing in the x-direction ($\delta x \approx 0.2$ mm) and to the absence of flow recirculation at the exit section. The exit condition $(\partial^2\phi/\partial \text{x}^2)|_{\text{out}} = 0$ was alternatively tested for $\phi = v$, T, k and $\tilde{\varepsilon}$, but it implied a much slower convergence rate and no significant changes were observed in the results.

3.2.3. Wall boundary conditions

The temperature value was specified on the isothermal solid walls, where the no-slip condition was assigned for velocity. The wall boundary conditions applied to k and $\tilde{\varepsilon}$ are specific of the version of the k–ε model used and are included in Table 2.

3.3. Numerical solution procedure

The partial differential equations were discretized using the finite volume method described in [24]. The convective fluxes at each control volume face were approached using the hybrid central/upward difference scheme. The velocities and pressures were iteratively calculated by the SIMPLEC algorithm, with the enhancements recommended in [25], and the discretized equations were solved by a tri-diagonal matrix algorithm. Calculations were performed on a 70×70 non-uniform staggered grid with 16 points in the jet inlet sections, where the first 'scalar' point was located at a wall distance of 0.09 mm (in the *test-case*, $x_{\text{n}_1}^+ < 0.45$ along all the walls). Numerical tests showed that this grid yielded nearly grid-independent solutions for the test-case, as compared to a 80×80 finer mesh. The criteria for convergence were: (i) normalized sum of

Table 2
Constants, wall-boundary conditions (BC) for k and $\tilde{\varepsilon}$, modifying functions and extra-terms for the turbulence models used in the present study: in model TH, the factor $[1-\exp(-Re_t^2)]$ in f_2 is applied only when $x_n^+ \leq 5$

Model	Code	$C_{\varepsilon 1}$	$C_{\varepsilon 2}$	$C_{\varepsilon 3}$	σ_k	k_w BC	$\tilde{\varepsilon}_w$ BC
Jones–Launder	JL	1.44	1.92	1.0	1.0	0	0
Launder–Sharma	LS	1.44	1.92	1.0	1.0	0	0
Nagano–Hishida	NH	1.45	1.9	1.0	1.0	0	0
Nagano–Tagawa	NT	1.45	1.9	1.0	1.4	$k_w=(\partial k/\partial x_n)_w=0$	$\nu(\partial^2 k/\partial x_n^2)$
Myong–Kasagi	MK	1.4	1.8	1.0	1.4	$k_w=(\partial k/\partial x_n)_w=0$	$\nu(\partial^2 k/\partial x_n^2)$
To–Humphrey	TH	1.44	1.92	$0.7/C_{\varepsilon 1}$	1.0	0	$2\nu(\partial\sqrt{k}/\partial x_n)^2$
Lam–Bremhorst	LB1	1.44	1.92	1.0	1.0	0	$(\partial\tilde{\varepsilon}/\partial x_n)_w=0$
Davidson	D	1.44	1.92	1.0	1.0	0	$(\partial\tilde{\varepsilon}/\partial x_n)_w=0$
Chieng–Launder (high-Re)	CL	1.44	1.92	1.0	1.0	$(\partial k/\partial x_n)_w=0$	$\tilde{\varepsilon}_1=2\nu k_1/x_{n_1}^2$

Code	f_μ	f_1	f_2	D_k	E_ε
JL	$\exp(\frac{-2.5}{1+Re_t/50})$	1	$1-0.3\exp(-Re_t^2)$	$-2\nu(\frac{\partial\sqrt{k}}{\partial x_j})^2$	$2\nu\nu_t(\frac{\partial^2 u_i}{\partial x_j\partial x_k})^2$
LS	$\exp[\frac{-3.4}{(1+Re_t/50)^2}]$	1	$1-0.3\exp(-Re_t^2)$	$-2\nu(\frac{\partial\sqrt{k}}{\partial x_j})^2$	$2\nu\nu_t(\frac{\partial^2 u_i}{\partial x_j\partial x_k})^2$
NH	$[1-\exp(\frac{-x_n^+}{26.5})]^2$	1	$1-0.3\exp(-Re_t^2)$	$-2\nu(\frac{\partial\sqrt{k}}{\partial x_j})^2$	$\nu\nu_t(1-f_\mu)(\frac{\partial^2 u_i}{\partial x_j\partial x_k})^2$
NT	$[1-\exp(-x_n^+/26)]^2\times(1+4.1/Re_t^{3/4})$	1	$\{1-0.3\exp[-(Re_t/6.5)^2]\}\times[1-\exp(-x_n^+/6)]^2$	0	0
MK	$[1-\exp(-x_n^+/70)]\times(1+3.45/Re_t^{1/2})$	1	$\{1-2/9\exp[-(Re_t/6)^2]\}\times[1-\exp(-x_n^+/5)]^2$	0	0
TH	$\exp(\frac{-2.5}{1+Re_t/50})$	1	$[1-0.3\exp(-Re_t^2)]\times[1-\exp(-Re_t^2)]$	0	0
LB1	$[1-\exp(-0.0165Re_n)]^2\times(1+20.5/Re_t)$	$1+(\frac{0.05}{f_\mu})^3$	$1-\exp(-Re_t^2)$	0	0
D	$\exp[\frac{-3.4}{(1+Re_t/50)^2}]$	$1+(\frac{0.14}{f_\mu})^3$	$[1-0.27\exp(-Re_t^2)]\times[1-\exp(-Re_n)]$	0	0
CL	1	1	1	0	0

the absolute residuals for the discretized equations $\leq 5\times10^{-5}$; (ii) maximum normalized iterative change of all variables $\leq 5\times10^{-5}$; (iii) relative iterative change of the outlet temperature $\leq 0.01\%$ and (iv) overall energy balance satisfied to within 0.05% of the thermal energy conveyed into the cavity by the jets.

3.4. Versions of k–ε turbulence model

Eight different versions of the low-Re k–ε model were considered for comparison, namely the models of Jones and Launder (JL) [19,20], Launder and Sharma (LS) [21], Lam and Bremhorst (LB) [26], To and Humphrey [27,28], Nagano and Hishida (NH) [29], Nagano and Tagawa (NT) [30], Myong and Kasagi (MK) [31] and Davidson (D) [10]. The constants, modifying functions and extra-terms that identify each version are listed in Table 2, together with the corresponding k and ε wall-boundary conditions. The values $C_\mu=0.09$ and $\sigma_\varepsilon=1.3$ were used for all models, following the original proposals; Pr_t and $C_{\varepsilon 3}$ were ascribed the constant values of 0.9 and 1.0, respectively, in all but model TH, where $C_{\varepsilon 3}=0.7/C_{\varepsilon 1}$ was used following its authors [28]. The original wall-boundary condition $\tilde{\varepsilon}_w = \nu(\partial^2 k/\partial x_n^2)$ proposed by Lam and Bremhorst [26] has been replaced here by $(\partial\tilde{\varepsilon}/\partial x_n)_w = 0$ (LB1), as adopted by Patel et al. [8].

Most of the above mentioned low-Re k–ε models were formerly proposed and tested for isothermal (LB1, NH, NT, MK) or forced convection (JL, LS) flows. Models TH and D were the only clearly designed by their authors for the numerical simulation of free and mixed convection flows, by incorporating the thermal buoyancy terms in the turbulence transport equations. In different ways, both were prepared to handle strong wall heat fluxes and large density variations. Model TH, in particular, is here represented in a rather reduced, simple form, if compared to the original one which included additional density fluctuation terms in the k and ε equations, in a variable-fluid-properties transient formulation. All low-Re k–ε models listed in Table 2 are nowadays called *conventional*, as they suffer from at least one of two drawbacks, only overcome by the most recent proposals

[32–35]: (i) only models NT and MK are able to reproduce the correct near-wall limiting behaviour of turbulence in the viscous sublayer of wall boundary layers, represented by $-\overline{u'v'} \propto x_n^3$, $\nu_t \propto x_n^3$, $k \propto x_n^2$ and $\varepsilon \to \varepsilon_w$ as $x_n \to 0$ [36]; (ii) models NH, NT and MK are subject to a singular problem thus leading to the prediction of an unrealistic local minimum of the wall heat transfer near points of flow reattachment.

In the present study, the dissipation variable $\tilde{\varepsilon}$ ($= \varepsilon + D_k$) was used in models JL, LS and NH throughout the calculation domain, without any restrictions. From the results given by these three models (e.g., vertical jet at $y/H = 0.5$ in the *test-case*), it was verified that the magnitude of the term D_k is significant only in the very near-wall region comprised in $0 < x_n^+ \leq 10$, where it was also observed that $(\partial\sqrt{k}/\partial x_n) \geq 0$. This is in agreement with the considerations found in recent studies, namely: $\tilde{\varepsilon}$ becomes identical to ε for $x_n^+ > 15$ [35], and $\tilde{\varepsilon}$ should be used as long as $(\partial\sqrt{k}/\partial x_n) \geq 0$, otherwise $D_k = 0$ [34].

It should be noticed that the high-*Re* form of the model equations is recovered for high turbulence Reynolds numbers Re_t, where functions f and the extra-terms D_k and E_ϵ reach their asymptotic values $f_\mu = f_1 = f_2 = 1$ and $D_k = E_\varepsilon = 0$. This can be seen in Table 2 for model CL, the so-called 'near-wall model for high Reynolds numbers' proposed by Chieng and Launder [3]. The corresponding two-layer wall-function procedure was here implemented with the simplifications referred in [5], namely the assumption that the turbulent energy and shear stress are essentially uniform over the fully turbulent flow region of the near-wall cell.

In this work, the calculations with the CL (high-*Re*) model were performed with the same fine grid in order to keep identical conditions for comparison with the other models. The major interest of this experience was to show that this model, without any 'low-*Re*' modifications except for the inclusion of the molecular diffusion term for all dependent variables, provided results with an overall equivalent quality. Using that fine grid, it was verified for the test-case configuration that all the wall-adjacent nodes lay well inside the viscous sublayer, where linear profiles for u and T prevail ($u^+ = y^+$, $T^+ = Pr\ y^+$). Under these conditions, the wall-functions derived from the logarithmic profiles of u and T were never activated, since only 'laminar' boundary conditions are needed for these variables (like with any low-*Re* turbulence model), together with the specifications of the k and ε boundary conditions listed in Table 2 and applicable for the viscous sublayer.

4. Characteristic parameters

The flow configuration considered in the present study is schematically represented in Fig. 1(b). Although mutually perpendicular, both air jets induce co-current moments of inertia that normally create a clockwise recirculating flow pattern inside the cavity. On the other hand, thermal buoyancy forces may act differently from one region to another in the flow domain. The balance between inertia and buoyancy forces may therefore vary significantly according to the local size and direction of both. In a mixed convection regime, this will be a decisive factor for the flow structure. The analysis should then involve the parameters that might be relevant for the description of such effects, either in local or in global terms.

It may be shown [37] that the present configuration of two buoyant jets emerging into a cavity with imposed temperature walls is completely defined by the following set of dimensionless parameters (cf. Fig. 1(b)): L/H, d/H, Re_h, Fr_h, Re_v/Re_h and Θ_w. Additionally, a global Froude number Fr_g and a global Reynolds number Re_g ($= Re_v + Re_h$) are convenient to represent the global relations of inertia to buoyancy, and inertial to viscous effects in the flow domain. The forced flow characteristic velocity U_c [$= (U_h + U_v)/2$, since $d_v = d_h = d$ in the studied cases] is used as a reference to represent the results for the velocity field.

5. Experimental results

5.1. Air inlet conditions: summary of the studied configuration

Local velocity and temperature measurements were made to characterize the air flow at the slot exits. The transverse profiles obtained at the symmetry plane of the model ($z/A = 0$) are plotted in Fig. 3(a), (b) for the horizontal and vertical jets, respectively. It may be seen that the normal component of the mean velocity in each jet is directed towards the respective adjacent wall. Unlike for temperature, the profiles of the streamwise mean velocity along each jet slot centerline present some asymmetries, as shown in Fig. 4. However, the two-dimensionality of each jet exit flow, over the central 90% of the test cavity width in the spanwise direction, lies within $\pm 10\%$ of the respective profile average value, u_m or v_m.

The deviations from u_m and v_m of the measured values at $z/A = 0$ were used to apply slight corrections to the profiles of the streamwise velocity component of Fig. 3(a), (b), thus giving the averaged jet discharge velocities: $U_h = 0.49$ m s^{-1} and $U_v = 0.59$ m s^{-1}. The

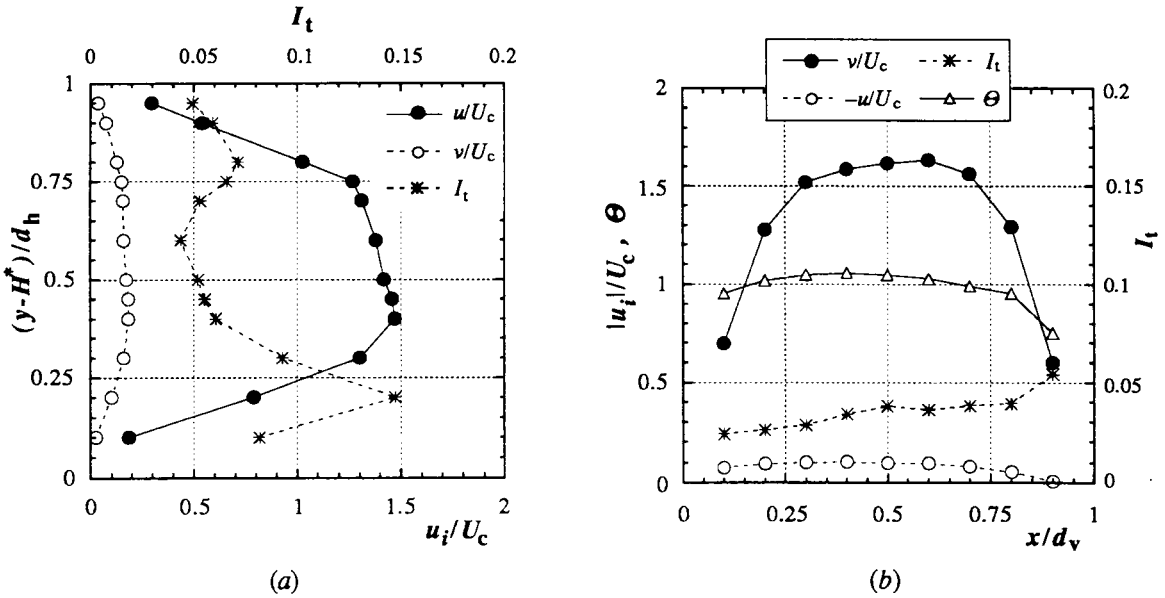

Fig. 3. Transverse profiles measured at $z/A = 0$ on the slot exits of the (a) horizontal and (b) vertical jets: streamwise [(a) u/U_c; (b) v/U_c] and normal [(a) v/U_c; (b) $-u/U_c$] mean-velocity components, turbulence intensity I_t and dimensionless temperature Θ ($H^* = H - d_h$; $U_c = 0.54$ m s^{-1}, $T_v = 35$°C, $T_h = T_w = 14$°C).

studied configuration (hereafter named *test-case*) is then defined by the following conditions: $L/H = 1$, $d/H = 1.92 \times 10^{-2}$, $Re_h = 623$, $Fr_h = 4.15$, $Re_v/Re_h = 1.215$, $\Theta_v = 1$ and $\Theta_h = \Theta_w = 0$. A corresponding Fr_g value of the order of unity (= 1.3, based on the mean outlet temperature $T_o = 19$°C) clearly indicates the presence of a mixed convection flow regime.

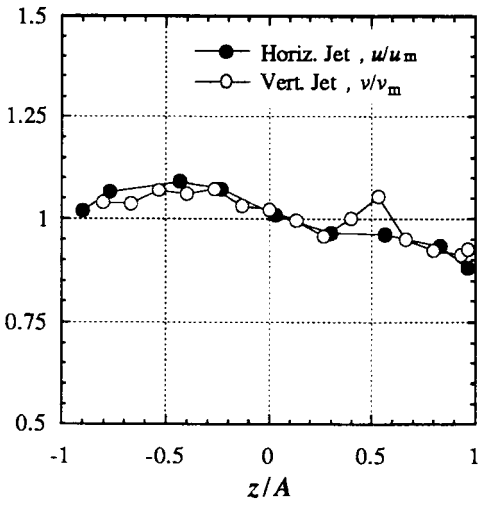

Fig. 4. Streamwise mean-velocity component measured along the exit slot centerline of each jet, normalized by the respective average value: $u_m = 0.74$ m s^{-1}, $v_m = 0.82$ m s^{-1}.

5.2. Flow structure and temperature distribution

Local measurements were made on the symmetry plane of the test cavity ($z/A = 0$) on a few hundreds of points distributed by Cartesian non-uniform grids of 17×20 and of 11×10 for velocity and temperature, respectively. As represented in Fig. 5, the flow structure is characterized by a well centered clockwise circulation, where no disturbance specifically due to the buoyancy forces is visible, in spite of the mixed convection regime. The air flow develops itself preferentially along the walls, and an important recirculating flow is evidenced by a meaningful value $U_{rm} = 0.46U_c$ near the floor and a rate of nearly three times that of the injected air flow. From Fig. 6(a), it can be concluded that the global level of turbulence intensity is independent of the quality of the flow at the jet inlet sections (for $I_{t_{in}} < 10\%$, see Section 3.2). It is rather determined by the turbulence shear production inside the cavity, particularly in the early mixing flow regions of the jets. Similar conclusions could be drawn for the temperature fluctuations (not shown here). On the other hand, the central region of the recirculating flow is characterized by low values of velocity ($< 0.2U_c$) and of turbulence intensity (5 to 10%). From the mean temperature distribution represented in Fig. 6(b), it is

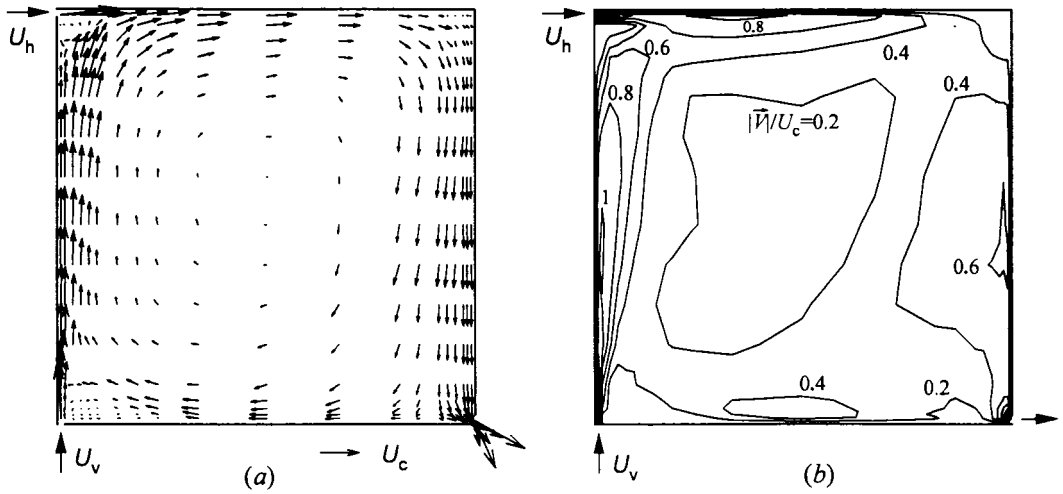

Fig. 5. Results from the local measurements of mean velocity in the symmetry plane ($z/A = 0$): (a) velocity vectors; (b) lines of isovalues of the velocity modulus ($U_c = 0.54$ m s^{-1}).

seen that most of the flow domain remains practically isothermal ($\Theta = 0.25$–0.3) and that the warm air issuing from the vertical jet reaches the top wall. Actually, the flow of the horizontal jet seems to be absent in the symmetry plane, since the velocity values are too low beneath the ceiling, where both jets should mix (see Fig. 5(b)). This suggests the presence of three-dimensional effects, which are pointed out in the z-profiles of the streamwise velocity component, shown in Fig. 7, measured at locations S_2 to S_5 (cf. Fig. 1(b)): deviations of up to 16% from the corresponding mean values, in the central 2/3 of the test cavity width. It is clear that the fluid flowing vertically (open symbols in Fig. 7) passes preferentially through the central region (between coordinates $z/A \approx \pm 0.5$), while the horizontal flows find a preferential path in the proximity of the guard walls ($z/A \approx \pm 1$). Except for the zone $z/A > 0.5$, the profiles at S_2 and S_3 (solid lines in Fig. 7) show opposite trends relatively to the corresponding mean values. Thus, it may be concluded that the development of the horizontal jet is strongly conditioned by the impact of the vertical jet flow: this latter is stronger in the central region, where it breaks down the momentum of the cold jet, which splits towards the guard walls. Such observations were confirmed by flow visualization, and explain the above mentioned vanishing of the cold jet in the symmetry plane.

Considering each profile at the locations S_i referred to in Fig. 7 (see also Fig. 1(b)), the deviation of the measured value at $z/A = 0$ from the profile z-averaged value u_m or v_m was adopted as a measure of the local defect of the flow from the desired two-dimensionality. Thus, in order to provide more accurate data for comparison with the 2D numerical calculations, such deviations were used to apply slight '2D corrections' to the profiles of the streamwise velocity measured in the symmetry plane and passing through those S_i locations. For example, the experimental values u_{exp} of the horizontal mean velocity component in Fig. 10(c) (beneath the ceiling at $x/L = 0.5$) include the following correction: $u_{exp} = u_{meas} \times f_{corr}$, where the correction factor was evaluated as $f_{corr} = (u_m/u_{z=0})$ from the u-profile along z shown in Fig. 7 for S_3.

6. Numerical results

In order to compare the performance of the different k–ε models listed above, each of them was used separately, assembled in the same 2D calculation program, to simulate the flow for the test-case configuration.

All models reproduce qualitatively the main features of the recirculating flow, as is exemplified in Figs. 8 and 9 with the solutions of model NH. However, some discrepancies are found if the different solutions are compared in detail. Except for models JL, LS and D, the predicted vertical velocity profiles near the left wall at $y/H = 0.5$ shown in Fig. 10(a) all exhibit a similar shape, and maximum values that differ by less than 16% from the maximum measured value (see Table 3). The calculated profiles in the vertical jet are thinner

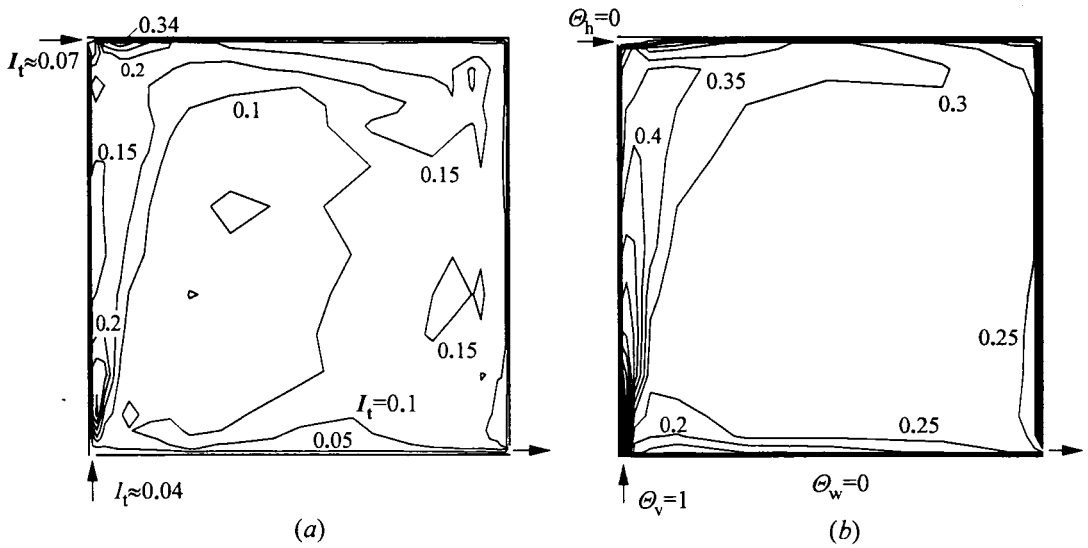

Fig. 6. Distributions of (a) turbulence intensity I_t and (b) dimensionless mean temperature Θ, from measurements in the symmetry plane of the test cavity.

than measured, thus indicating a greater laboratory jet spreading rate in the symmetry plane.

Considering the turbulent viscosity in the near-wall region of the vertical jet (e.g. $x^+ \leq 30$–40, see Fig. 10(d)), the tested models can be cast into three groups. Models CL, NH and TH predict intermediate values of ν_t, which are likely to be the best approaches in this region of the flow. On the other hand, models JL and LS clearly overpredict the turbulent diffusion in the near-wall region (e.g., at $x^+ \approx 10$, given by LS is 6 to 7 times greater than that given by model NH); consequently, the corresponding velocity and temperature profiles in the development regions of the wall jets are flattened, showing too low peak values (see Fig. 10(a)–(c)), while wall heat losses are overestimated, resulting in a too low temperature level in the almost isothermal core (see Fig. 11). This tendency of model LS has been observed by other authors in wall heat or mass transfer problems, either in natural [12,38] or forced convection flows [13,39]. The addition of an extra source term in the ε equation—the so-called *Yap correction* [5]—is recommended as a remedy to ensure a correct level of the dissipation length scales near the wall. Finally, in contrast with JL and LS, the turbulent diffusion in the near-wall region is rather underestimated by models LB1, NT, MK and, most seriously, by model D, in which case the flow remains practically laminar across the whole inner layer of the jet (i.e., $x/L < 0.006$), thus leading to too sharp velocity and temperature profiles. Except for this last group, all models present profiles of the turbulence intensity—qualitatively equivalent to those of k, since $k \propto I_t^2$—with two peak values, one in the inner layer and the other in the outer layer of the vertical jet. The inter-

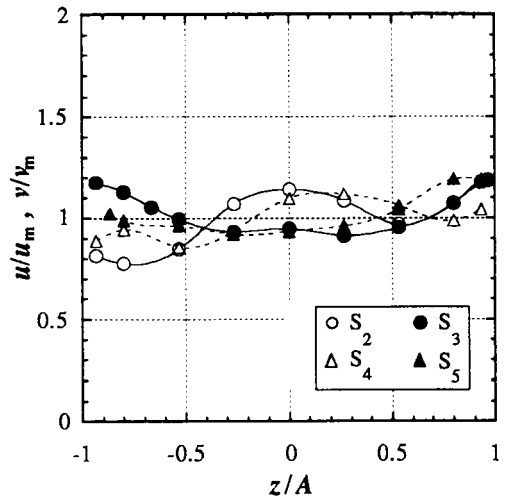

Fig. 7. Profiles of the streamwise velocity component measured along the z-direction at stations S_2–S_5 (see Fig. 1(b)) and normalized by the corresponding mean value, u_m or v_m (solid and open symbols are used for u and v, respectively).

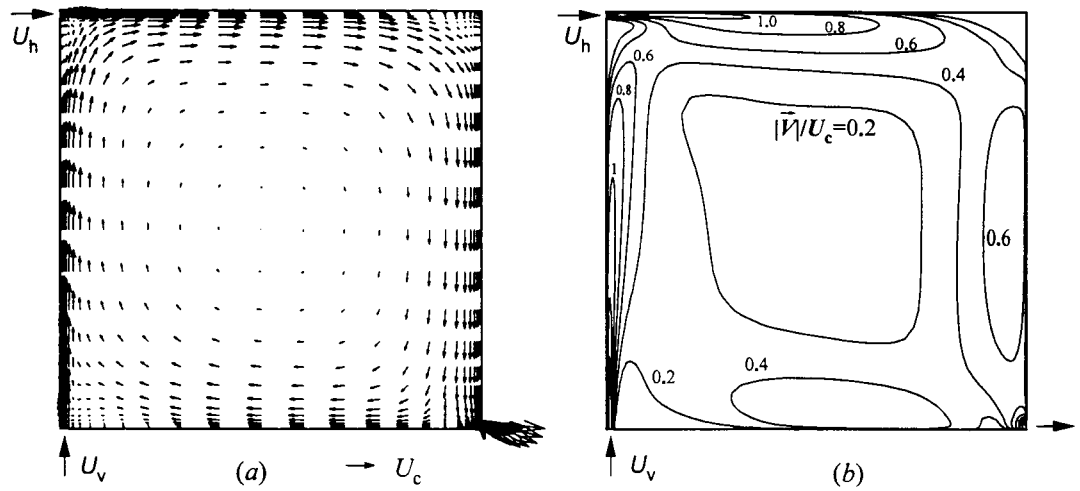

Fig. 8. Numerical results obtained with model NH: (a) velocity vectors plotted on every two grid nodes; (b) isovalues of the velocity modulus ($U_c = 0.54$ m s^{-1}).

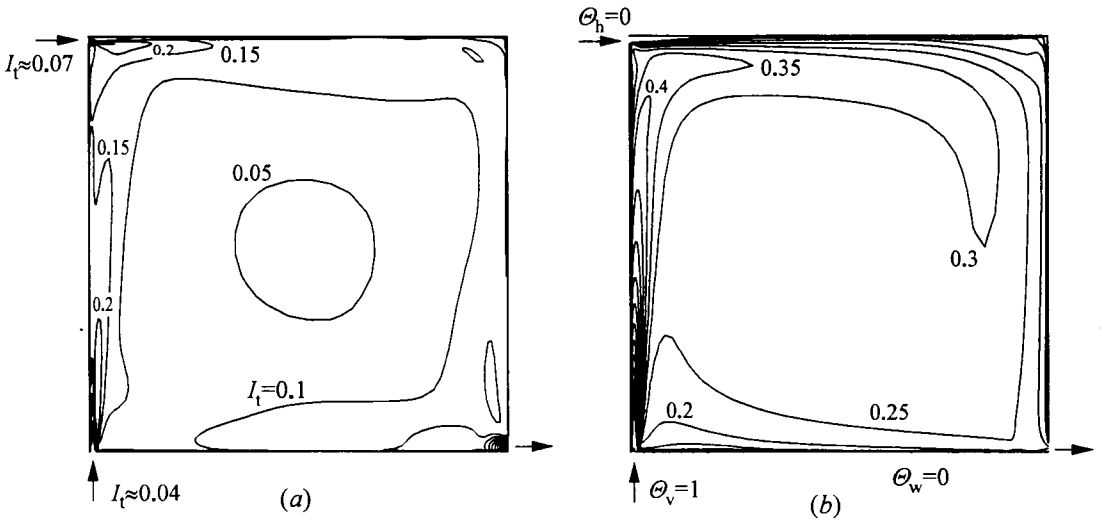

Fig. 9. (a) Isovalues of turbulence intensity [$I_t = (2k/3)^{1/2}$] and (b) of dimensionless mean temperature, as calculated with model NH.

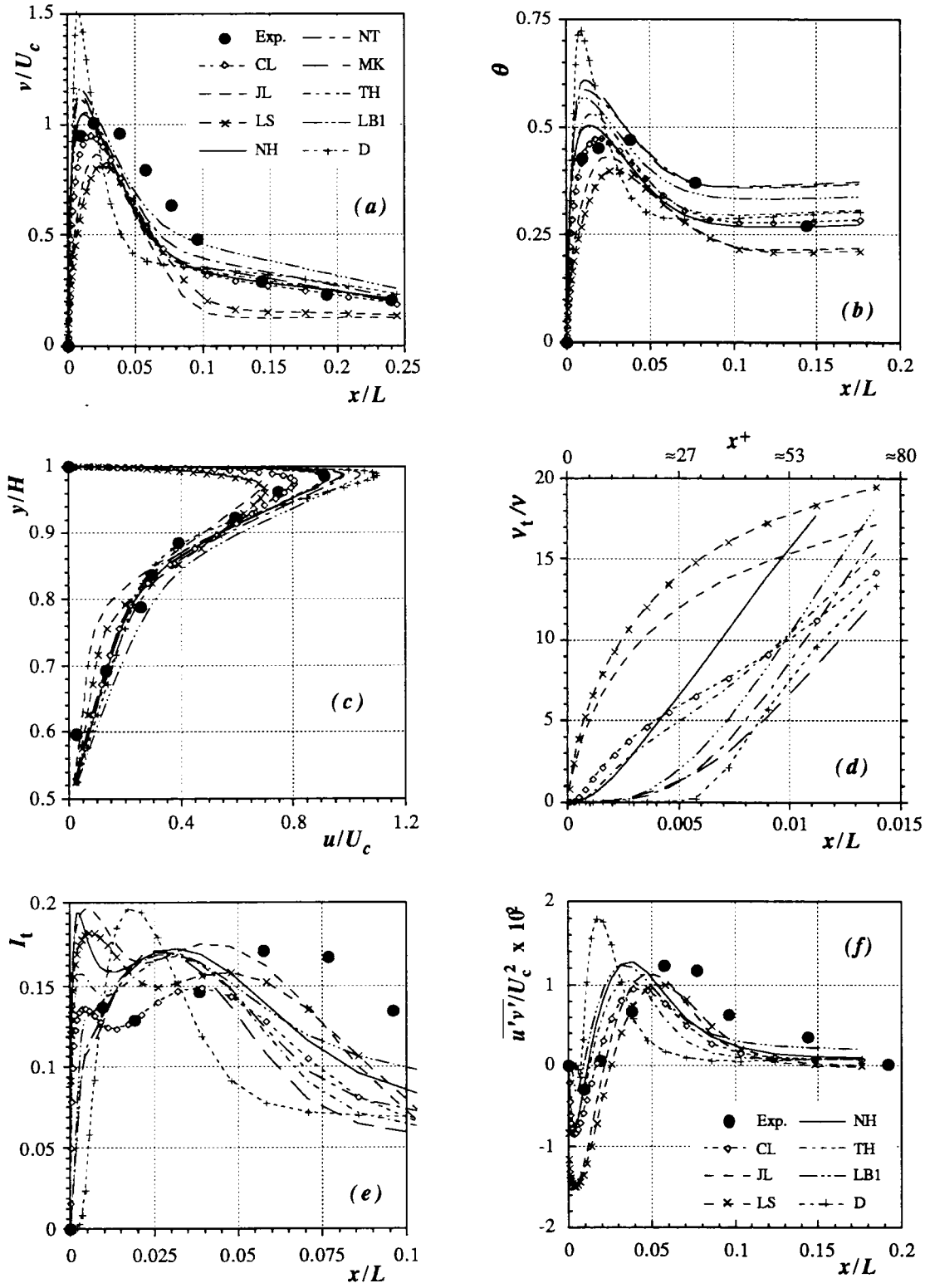

Fig. 10. Comparison of the results obtained with the different versions of the k–ε model. Transversal profiles in the wall jets: (a) vertical velocity component and (b) temperature, at $y/H = 0.5$; (c) horizontal velocity under the ceiling, at $x/L = 0.5$; (d) turbulent viscosity, (e) turbulence intensity and (f) turbulent shear stress, at $y/H = 0.5$.

Table 3
Particular values of some representative profiles: maxima of (a) vertical velocity at $y/H = 0.5$; (b), (c) horizontal velocity at $x/L = 0.5$, in the upper and lower halves of the cavity, respectively; (d) maximum temperature at mid-height and (e) temperature at the center; (f) average Nusselt number on the left wall: $U_c = 0.54$ m s^{-1}; ▲: experimental values after 2D correction

	(a) $\{v_{max}/U_c\}_{Left}$	(b) $\{u_{max}/U_c\}_{Up}$	(c) $\{u_{max}/U_c\}_{Down}$	(d) $\{\Theta_{max}\}_{Left}$	(e) Θ_{Center}	(f) $\overline{Nu}_{Left}$
Exp.	1.006	0.913 (▲)	0.437 (▲)	0.471	0.267	–
JL[a]	−14.1%	−24.5%	−25.8%	−8.5%	−10.5%	295.5
LS	−18.8%	−23.3%	−12.6%	−15.3%	−14.1%	295.0
NH	+3.6%	+1.1%	+10.1%	+6.8%	+7.3%	191.7
NT	+10.6%	+7.8%	+35.5%	+24.3%	+41.0%	146.1
MK	+13.3%	+7.1%	+31.9%	+29.0%	+42.9%	151.8
TH	+4.6%	−0.1%	+22.9%	+12.2%	+17.9%	204.3
LB1	+15.0%	+14.2%	+45.2%	+20.4%	+30.0%	151.9
D	+50.6%	+20.4%	+22.7%	+53.7%	+17.2%	158.4
CL	−5.6%	−11.1%	+14.7%	+0.5%	+10.4%	234.7
NH(Pr_t,$C_{\varepsilon 3}$)$_{var}$	+5.3%	+1.1%	+18.0%	+0,7%	+1.3%	185.9
LS + corr. Yap	−1.9%	−6.3%%	+13.8%	+4.2%	+18.4%	207.5

[a] See model codes in Table 2.

mediate minimum occurs around the location of maximum velocity (Fig. 10(e)), which is in general agreement with the shape of the measured profile at $y/H = 0.5$. As is typical for wall jet flows [40,41], it was experimentally observed that this is also the shape of the streamwise velocity fluctuation profiles along the region comprised from $y/d = 15$–35 of the vertical jet, in contrast with the normal velocity fluctuations, which present only the second peak at about the same distance from the wall.

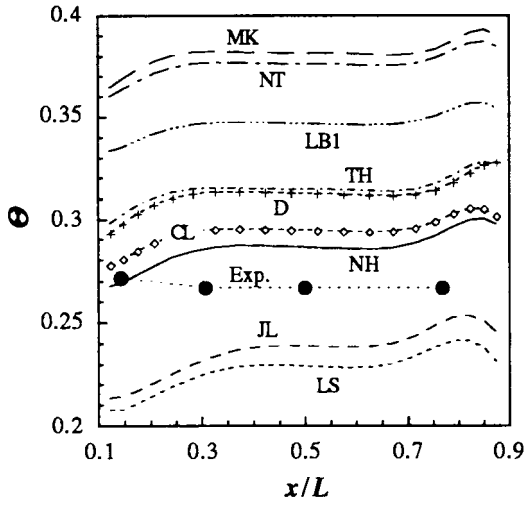

Fig. 11. Horizontal profiles of the measured and calculated mean temperature in the central region at mid-height of the cavity ($y/H = 0.5$).

It is also noteworthy that, except for model D, all the tested models predict normal distributions of the turbulent shear stress $\overline{u'v'}$ that qualitatively agree with the typical behaviour for wall jet flows [40,41] (see Fig. 10(f)). In all of them, $\overline{u'v'}$ passes from negative to positive slightly closer to the wall than the corresponding location of maximum velocity. Again, the overestimation by models JL and LS of the turbulent momentum diffusion in the inner layer of the jet becomes evident. In spite of the deficient experimental information in the immediate vicinity of the wall, Fig. 10(f) allows to conclude that models CL, TH and NH produce reasonable approximations to the normal distribution of $\overline{u'v'}$, particularly if the generally wider shape of the measured profiles for the vertical jet in the symmetry plane is considered.

The profiles of the local Nusselt number along the cavity walls, taken from the different numerical solutions, are plotted in Fig. 12. Apart from local details in regions of separated flow, discrepancies between them are more evident on the left wall. Particularly around its mid-height, the curves may be grouped into three sets, just like the profiles of ν_t in Fig. 10(d), showing the direct relation between the turbulent diffusion in the jet inner layer and the heat transfer to the wall. Since the left wall is responsible for 50–70% of the total heat transfer, the profiles of Nu in Fig. 12(a) and their average values in Table 3(f) are also closely related to the different calculated values for the

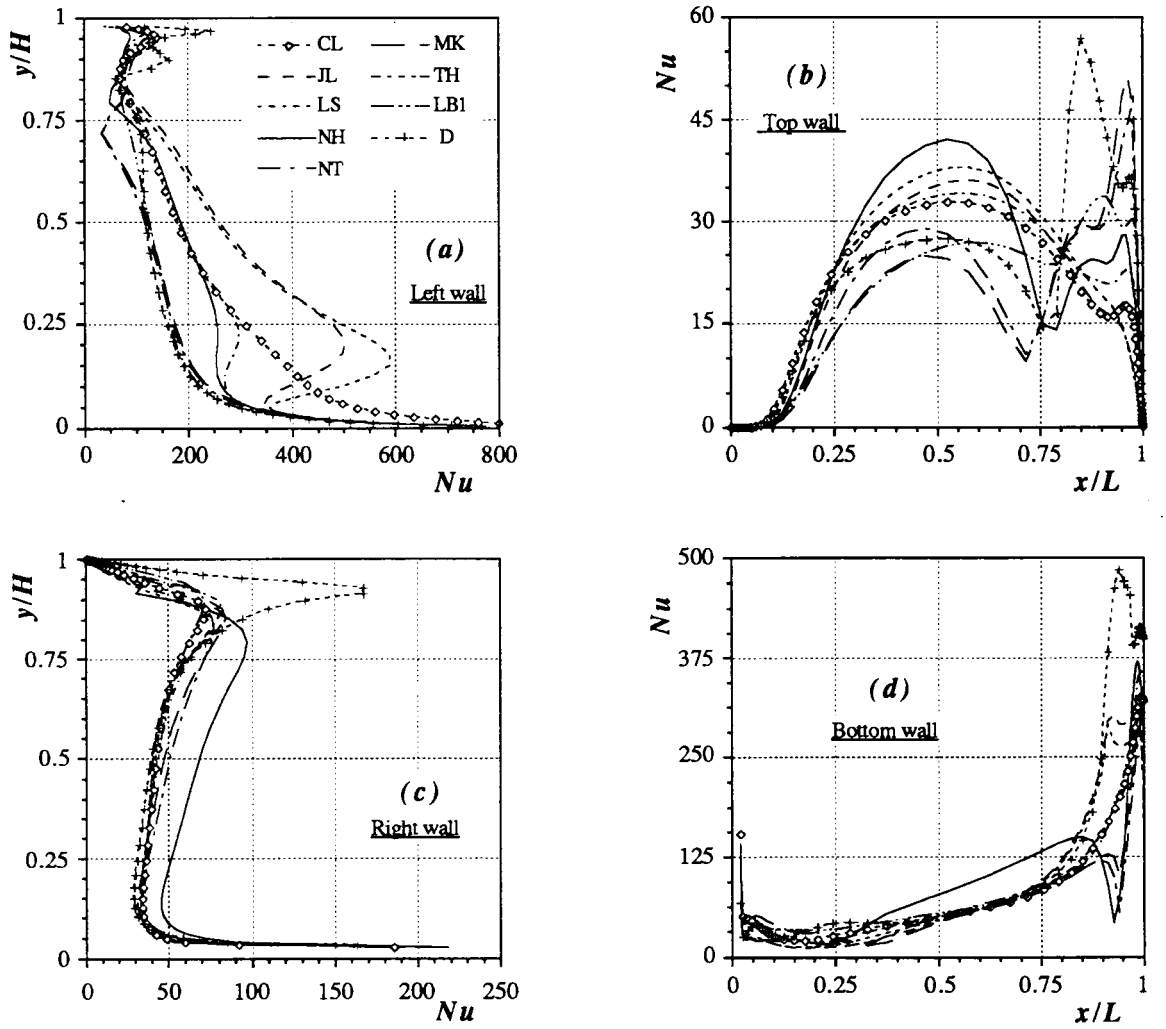

Fig. 12. Profiles of the local Nusselt number along the walls, after the prediction with the different versions of the k–ε model.

temperature level at the cavity center (see Fig. 11 and Table 3). Actually, in the absence of experimental data for the wall heat fluxes, this parameter was selected as indicative of the global performance of the different turbulence models to evaluate the wall heat transfer in the present configuration. It may thus be concluded that wall heat fluxes are most underestimated by models MK, NT and LB1, by the same decreasing order as they underpredict the turbulent diffusion in the near-wall region (Fig. 10(d)). For model D, this effect is globally attenuated, because it significantly overpredicts the wall heat transfer in the regions of separated flow (upper right corner, Fig. 12(b), (c)) and reattaching flow (Fig. 12(d)). On the other hand, as expected, the wall heat fluxes are overestimated by models JL and LS, leading to a too low temperature level at the cavity center.

Fig. 12(b)–(d) show that, as compared to the others, model NH tends to somehow overpredict the heat transfer to the walls in the regions of attached flow. However, in the present configuration, this feature seems to contribute to a better approach for the corresponding predicted temperature at the center. The local minima of the Nusselt number given by models NH, NT and MK on the bottom wall (Fig. 12(d), $x/L \approx 0.9$) are unrealistic. They illustrate the so-called

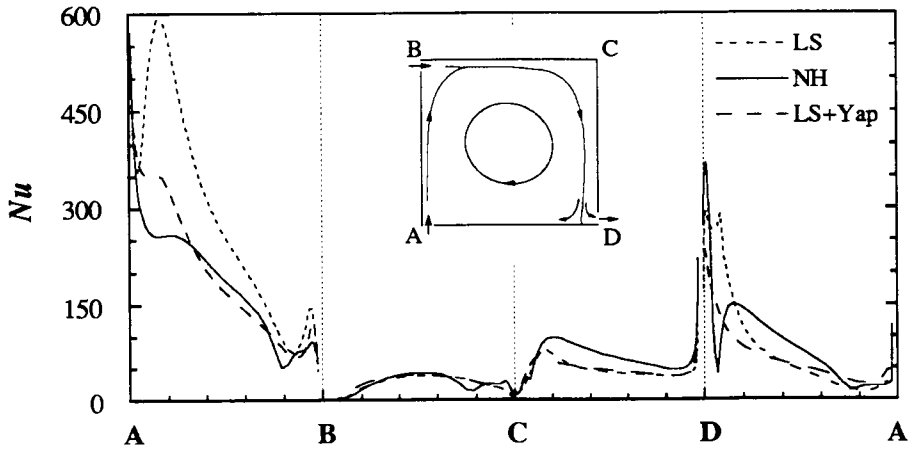

Fig. 13. Effect of the Yap correction on the prediction with model LS for the local Nusselt number along the four walls. Results with model NH were kept for reference.

singularity problem, which is common to all low-*Re* k–ε models where the damping function f_μ depends on the wall shear stress τ_w (implicitly through the definitions of x_n^+ and u_τ), going to zero at a point of separating or reattaching flow. Consequently, the turbulent viscosity calculated on a grid line passing through such a point will always come out null regardless of the wall distance, which is physically impossible. Anyway, in the context of the overall flow pattern, the importance of such singularity defects will depend on the relative extent of the regions of separated flow, together with other factors: resolution of the numerical grid parallel to the wall; possible coincidence of a grid line with those physical singularities of the flow; proximity of another wall; etc. New versions of the low-*Re* k–ε model have been more recently proposed [32–35], that eliminate this singularity problem, but still remain to be tested in this class of confined mixed convection flows.

Fig. 13 shows the effect of the Yap correction on the local Nusselt number predicted along the four walls with model LS. Drastic reductions of the wall heat transfer are observed along the vertical warm jet, as well as near the flow reattachment on the bottom wall, thus indicating a reduction of the predicted near-wall turbulent diffusion at those regions. The overall effect—a 22% global reduction—seems however exaggerated, since the resulting central temperature becomes too high (see Table 3). Other effects of the Yap correction are also presented in Table 3, meaning significant improvements in the velocity and temperature profiles of the vertical jet, in which inner layer the turbulent viscosity came to a level comparable to that of model NH. On the other hand, the effect on *Nu* of using variable Pr_t and $C_{\varepsilon 3}$ with model NH (see below) is negligible and was omitted in Fig. 13.

From the above considerations, particularly those relative to Figs. 10 and 11, and Table 3, it may be concluded that the best overall agreement with experiments is achieved with the model of Nagano and Hishida [29]. The good overall quality of the results provided by the model of CL in the same near-wall refined grid (no active log-law wall-functions) should be pointed out, especially taking into account that it is not conceptually recommended for low turbulence flows, nor to solve the turbulence transport equations all the way to the walls, through the viscous sublayer. This model can be here elected as the second best performing one, ahead of most low-*Re* turbulence models including the one of TH.

It should be emphasized that the adequacy of the above models is however strongly problem dependent. With the boundary conditions of the experiment reported in [16], they were all compared to simulate a mixed convection flow configuration with a single horizontal, cold jet near the ceiling and heat being supplied to the flow by the heated floor of the cavity. In this case, the models of LB1 and NT provided the best agreement with the measured temperature field, by correctly predicting the experimental value at the isothermal core, while the models of NH, JL and LS overestimated the wall heat transfer rate yielding too high temperature values at the center.

Improvements of the results with the model of NH

were still achieved by two further assumptions: (i) a variable turbulent Prandtl number, according to the expression suggested in [42],

$$Pr_t = \frac{\kappa[1-\exp(-x_n^+/A^+)]}{\kappa'[1-\exp(-x_n^+/B^+)]} \quad (6)$$

where $A^+ = 26$, as in the original proposal, and the values $B^+ = 50$ and $\kappa' = \kappa/0.55$ were optimized to better approximate the measured temperature field; and (ii) the 'constant' $C_{\varepsilon 3}$ varying locally with the direction of the mean-velocity vector as used by Henkes [9]: $C_{\varepsilon 3} = \tanh|v/u|$. By this way, the deviations of $\{\theta_{max}\}_{Left}$ and θ_{Centre} from experiments were reduced to 0.7% and 1.3%, respectively, with no significant changes in the flow field (see Table 3).

7. Conclusions

The mixed convection, nominally two-dimensional airflow generated by two non-isothermal plane wall jets inside a cavity has been investigated both experimentally and numerically. Experimental data are reported of the velocity and the temperature turbulent fields in the symmetry plane of a 1×1 m^2 cross-section cavity. Taking these as a basis, the numerical predictions obtained with nine different formulations of the k–ε turbulence model were comparatively analysed for validation purposes.

It was found that, particularly in the domain of the wall jets, the low-Reynolds-number model of Jones and Launder [19,20], and its extension by Launder and Sharma [21] produce too high levels of turbulence energy in the near-wall region, thereby overestimating the wall heat fluxes. On the contrary, the models of Myong and Kasagi [31], of Nagano and Tagawa [30] and of Lam and Bremhorst [26], in this decreasing order, underpredict the wall heat fluxes. A rather satisfactory performance was achieved with a simplified, yet consistent formulation of the 'near-wall model for high Reynolds numbers' of Chieng and Launder [3,5] (model CL), which, in the same fine grid, did not make use of the inherent log-law wall-functions. However, although suffering from singular defects occurring near separation/reattachment points of the flow, the low-Re model of Nagano and Hishida [29] provided the best overall approach to the experimental data for the tested configuration. The results with this model were still improved by varying the turbulent Prandtl number, Pr_t, and the 'constant' $C_{\varepsilon 3}$, in the ε equation, according to appropriate functions. This methodology was thus selected to be subsequently explored in systematic calculations for a parametric study of this type of confined two-jet flow problem, the results of which will be reported in the near future.

Finally, it should be mentioned that universality can not be claimed for the conclusions of the present validation study, since the performance of the investigated models is problem dependent and particularly sensitive to the extent and location of regions of unstable thermal stratification. The authors acknowledge the limitations of the present experimental results, mainly due to the lack of measurements in the near-wall regions and to deviations from two-dimensionality of the laboratory modelled flow, which were somehow reduced by the application of '2D corrections'. The present study could be usefully extended to other flow configurations, e.g., the forced convection flow over a backward-facing step and the natural convection within a rectangular cavity with differentially heated vertical walls.

Acknowledgements

The experiments reported in the present work were conducted in the Laboratoire d'Etudes Thermiques of the University of Poitiers and were supported by the Department of Electricity Applications of Electricité de France. The cooperation between the Universities of Coimbra and Poitiers was supported by the Portuguese and French Governments, through the Instituto Nacional de Investigação Científica and the Ambassade de France au Portugal.

References

[1] Q. Chen, Z. Jiang, Significant questions in predicting room air motion, ASHRAE Trans. 98 (1) (1992) 929–939.
[2] B.E. Launder, D.B. Spalding, The numerical computation of turbulent flows, Comp. Meth. Appl. Mech. Engng. 3 (1974) 269–289.
[3] C.C. Chieng, B.E. Launder, On the calculation of turbulent heat transport down-stream from an abrupt pipe expansion, Numer. Heat Transfer 3 (1980) 189–207.
[4] N. Djilali, I. Gartshore, M. Salcudean, Calculation of convective heat transfer in recirculating turbulent flow using various near-wall turbulence models, Numer. Heat Transfer, A 16 (1986) 189–212.
[5] B.E. Launder, On the computation of convective heat transfer in complex turbulent flows, J. Heat Transfer 110 (1988) 1112–1128.
[6] M. Ciofalo, M.W. Collins, k–ε predictions of heat transfer in turbulent recirculating flows using an improved

wall treatment, Numer. Heat Transfer, B 15 (1989) 21–47.
[7] S. Thangam, C.G. Speziale, Turbulent separated flow past a backward-facing step: critical evaluation of two-equation turbulence models, AIAA J. 30 (1992) 1314–1320.
[8] V.C. Patel, W. Rodi, G. Scheuerer, Turbulence models for near-wall and low-Reynolds number flows: a review, AIAA J. 23 (1985) 1308–1318.
[9] R.A. Henkes, Natural-convection boundary layers. PhD thesis, Faculty of Applied Physics, Delft University of Technology, The Netherlands (1990).
[10] L. Davidson, Calculation of the turbulent buoyancy-driven flow in a rectangular cavity using an efficient solver and two different low Reynolds number k–ε turbulence models, Numer. Heat Transfer, A 18 (1990) 129–147.
[11] F.B. Cheung, D.Y. Sohn, Numerical study of turbulent natural convection in an innovative air cooling system, Numer. Heat Transfer, A 16 (1989) 467–487.
[12] N.Z. Ince, B.E. Launder, Three-dimensional and heat-loss effects on turbulent flow in a nominally two-dimensional cavity, Int. J. Heat Fluid Flow 16 (1995) 171–177.
[13] H. Ramamurthy, S. Ramadhyani, R. Viskanta, A study of low-Reynolds-number k–ε turbulence models for radiant-tube applications, J. Institute of Energy 66 (1993) 188–197.
[14] W.D. Hsieh, K.C. Chang, Calculation of wall heat transfer in pipe-expansion turbulent flows, Int. J. Heat Mass Transfer 39 (1996) 3813–3822.
[15] Q. Chen, Comparison of different k–ε models for indoor air flow computations, Numer. Heat Transfer, B 28 (1995) 353–369.
[16] D. Blay, S. Mergui, C. Niculae, Confined turbulent mixed convection in the presence of a horizontal buoyant wall jet, in: Fundamentals of Mixed Convection, Trans. ASME, HTD-Vol. 213, 1992, pp. 65–72.
[17] Guidelines for Ventilation Requirements in Buildings, Report no. 11, European Concerted Action—Indoor Air Quality and Its Impact on Man, Commission of the European Communities, 1992.
[18] J.J. Costa, S. Mergui, J.L. Tuhault, F. Penot, D. Blay, L.A. Oliveira, Test of turbulence models for the numerical simulation of internal mixed convection flows, in: Proceedings ROOMVENT'92—Third International Conference on Air Distribution in Rooms, Aalborg, Denmark, vol. 1, 1992, pp. 159–175.
[19] W.P. Jones, B.E. Launder, The prediction of laminarization with a two-equation model of turbulence, Int. J. Heat Mass Transfer 15 (1972) 301–314.
[20] W.P. Jones, B.E. Launder, The calculation of low-Reynolds number phenomena with a two-equation model of turbulence, Int. J. Heat Mass Transfer 16 (1973) 1119–1130.
[21] B.E. Launder, B.I. Sharma, Application of the energy-dissipation model of turbulence to the calculation of flow near a spinning disk, Lett. Heat Mass Transfer 1 (1974) 131–138.
[22] J.J. Costa, D. Blay, L.A. Oliveira, Numerical study of the turbulent mixed convection flow generated by two non-isothermal plane jets in a compartment, in: Proceedings ROOMVENT'94—Fourth International Conference on Air Distribution in Rooms, 15–17 June, Kraków, Poland, vol. 1, 1994, pp. 575–593.
[23] D.D. Gray, A. Giorgini, The validity of the Boussinesq approximation for liquids and gases, Int. J. Heat Mass Transfer 19 (1976) 545–551.
[24] S.V. Patankar, Numerical Heat Transfer and Heat Flow, McGraw-Hill, New York, 1980.
[25] J.P. Van Doormaal, G.D. Raithby, Enhancements of the SIMPLE method for predicting incompressible fluid flows, Numer. Heat Transfer 7 (1984) 147–163.
[26] C.K.G. Lam, K. Bremhorst, A modified form of the k–ε model for predicting wall turbulence, J. Fluids Engng. 103 (1981) 456–460.
[27] W.M. To, J.A.C. Humphrey, Numerical simulation of buoyant, turbulent flow—I: free convection along a heated, vertical, flat plate, Int. J. Heat Mass Transfer 29 (1986) 573–592.
[28] J.A.C. Humphrey, W.M. To, Numerical simulation of buoyant, turbulent flow—II: free and mixed convection in a heated cavity, Int. J. Heat Mass Transfer 29 (1986) 593–610.
[29] Y. Nagano, M. Hishida, Improved form of the k–ε model for wall turbulent shear flows, J. Fluids Engng. 109 (1987) 156–160.
[30] Y. Nagano, M. Tagawa, An improved k–ε model for boundary layer flows, J. Fluids Engng. 112 (1990) 33–39.
[31] H.K. Myong, N. Kasagi, A new approach to the improvement of k–ε turbulence model for wall-bounded shear flows, JSME Int. J., Series II 33 (1990) 63–72.
[32] K.C. Chang, W.D. Hsieh, C.S. Chen, A modified low-Reynolds-number turbulence model applicable to recirculating flow in pipe expansion, J. Fluids Engng. 117 (1995) 417–423.
[33] K. Abe, T. Kondoh, T. Nagano, A new turbulence model for predicting fluid flow and heat transfer in separating and reattaching flows—II: thermal field calculations, Int. J. Heat Mass Transfer 37 (1995) 1467–1481.
[34] Y. Nagano, M. Shimada, Development of a two-equation heat transfer model based on direct simulations of turbulent flows with different Prandtl numbers, Phys. Fluids 8 (12) (1996) 3379–3402.
[35] C.B. Hwang, C.A. Lin, Improved low-Reynolds-number k–$\tilde{\varepsilon}$ model based on direct numerical simulation data, AIAA J. 36 (1) (1998) 38–43.
[36] D.R. Chapman, G.D. Kuhn, The limiting behaviour of turbulence near a wall, J. Fluid Mechanics 170 (1986) 265–292.
[37] J.J. Costa, Study of the flow generated by two non-isothermal wall jets in a closed domain. PhD thesis (in Portuguese), Dept. Mech. Engng., University of Coimbra, Portugal, 1996.
[38] P.L. Betts, Dafa'Alla AA Turbulent buoyant air flow in a tall rectangular cavity, in: Significant Questions in Buoyancy Affected Enclosure or Cavity Flows, HTD-60, ASME Winter Annual Meeting, Anaheim, 1986, pp. 83–91.
[39] S. Nesić, J. Postlethwaite, D.J. Bergstrom, Calculation of wall-mass transfer rates in separated aqueous flow using a low Reynolds number k–ε model, Int. J. Heat Mass Transfer 35 (1992) 1977–1985.

[40] H.P.A.H. Irwin, Measurements in a self-preserving plane wall jet in a positive pressure gradient, part I, J. Fluid Mech. 61 (1973) 33–63.
[41] I. Wygnanski, Y. Katz, E. Horev, On the applicability of various scaling laws to the turbulent wall jet, part I, J. Fluid Mech. 234 (1992) 669–690.
[42] T. Cebeci, A. Khattab, Prediction of turbulent-free-convective-heat transfer from a vertical flat plate. J. Heat Transfer (1975) 469–471.